Spherical gravitational wave antennas and the truncated icosahedral arrangement

Stephen M. Merkowitz and Warren W. Johnson

Department of Physics and Astronomy, Louisiana State University, Baton Rouge, Louisiana 70803

A spherical gravitational wave detector can be equally sensitive to a wave from any direction, and also can be able to measure its direction and polarization. We derive a set of equations to describe the mechanics of a spherical antenna coupled to an arbitrary number of attached mechanical resonators. A special arrangement of six resonators is proposed, which we term a truncated icosahedral gravitational wave antenna. An analytic solution to the equations of motion is found for this case. We find that direct deconvolution of the gravitational tensor components can be accomplished with a specified set of linear combinations of the resonator outputs, which we call the mode channels. We develop one simple noise model for this system and calculate the resulting strain noise spectrum. We conclude that the angle-averaged energy sensitivity will be 56 times better than for the typical equivalent bar-type antenna with the same noise temperature.

I. INTRODUCTION

Confirmed detection of gravitational waves from astrophysical sources will found a new astronomy and allow direct investigation of the gravitational force under extreme conditions. The best current antennas, such as the LSU ALLEGRO detector [1], are sensitive enough to detect a gravitational collapse in our Galaxy, if the energy converted is a few percent of a solar mass. However, the conventional wisdom is that we need to look at least 3 orders of magnitude further in distance, out to the Virgo Cluster, to have an "assured" event rate of several per year. This requires improving the energy resolution of the detector by 6 orders of magnitude. The best known methods for improving cryogenic resonant-mass detectors will contribute by lowering the noise temperature T_n from its current value of ≈ 7 mK. It is commonly believed that quantum noise will present a formidable barrier for improvement by more than 10^5, not quite enough for "assured" detection.

There are other ways to improve resonant-mass antennas that are independent of the noise temperature. One way is to increase the cross section of the antenna. Another is to construct many antennas, each aimed in a different direction, so every source direction and polarization will be in the most sensitive part of at least one antenna pattern. This method adds the ability to determine source direction and polarization. A "spherical" antenna will provide all three advantages in a single instrument. We use the word "spherical" for any shape that approximates a true sphere and has equivalent quadrupole vibrational modes.

The important question becomes the following: What quantitative improvement can a sphere actually deliver? We have invented a design for a nearly spherical antenna, which we call a truncated icosahedral gravitational wave antenna (TIGA) that provides an elegant solution to certain complications of a spherical antenna, and lets us calculate the quantitative improvement. We conclude that

a TIGA will be about 56 times more sensitive in energy than the typical equivalent bar-type antenna with the same noise temperature T_n. Combined with a quantum limited T_n, this is a sufficient factor to increase our range by more than the desired factor. If we further assume construction of a set of detectors for different frequencies (a "xylophone"), the sensitivity is further improved and waveform information can be obtained.

It was recognized long ago [2] that a sphere is a very natural shape for a resonant-mass detector of gravitational waves. A free sphere has five degenerate quadrupole modes of vibration that will interact strongly with a gravitational wave. Each free mode can act as a separate antenna, oriented toward a different polarization or direction. Wagoner and Paik [3] found a set of equations to determine the source direction in the celestial hemisphere from the free mode amplitudes. They also calculated the angle-averaged energy absorption cross section of a sphere. Compared to a bar with the same quadrupole mode frequency and a typical length to diameter ratio of 4.2, the improvement in cross section is about a factor of 60.

That result was ignored, perhaps because a simple spherical resonator is not a practical detector. One requirement for practicality is a set of secondary mechanical resonators. All successful cryogenic bar-type detectors have such resonators; they act as mechanical-impedance transformers between the primary vibrational modes of the antenna and the actual motion sensors, producing an essential increase in the electromechanical coupling. We expect that a sphere with five primary modes will require at least five secondary resonators. Another requirement is a clear method for spatial deconvolution of the signal, so we can determine its direction and polarization. A third requirement is a way to quantify the noise when multiple motion sensors are used.

It is not hard to imagine that the presumed advantages of a sphere may be lost due to these practical requirements. In order to determine the feasibility of a spher-

ical antenna, the complications of extra modes needs to be addressed. Our analysis is an extension to multimode antennas of the type used by Michelson and Taber to discuss a bar antenna with a single secondary resonator [4,5].

We present here detailed calculations for the sensitivity of a spherical detector for a case where the secondary resonators have a particular useful symmetry. A brief review of some of these results has been previously published [6].

We begin by introducing the quadrupolar decomposition of the gravitational field in Sec. II. Section III reviews the fundamental mechanical equations and the eigenfunction expansion for a general antenna. Section IV reviews the quadrupolar eigenfunctions for a sphere and shows that they exactly match the quadrupolar decomposition of the gravitational field. A derivation of a general model for coupling resonators to a sphere is presented in Sec. V. A special geometry (the "TIGA configuration") is introduced that simplifies the behavior of the coupled system, and allows us to obtain a general analytic solution. A direct, one-to-one, readout for each of the quadrupolar components of the gravitational field is provided by a linear combination of the resonator outputs, called "mode channels." The behavior of the complete system is illustrated with a numerical simulation of its response to waves with different directions and polarizations. Section VI develops a simple noise model, and calculates the resulting "spectral sensitivity" of the detector. Section VII compares the spectral sensitivities of several detectors.

II. QUADRUPOLE DECOMPOSITION OF THE GRAVITATIONAL FIELD

A gravitational wave is a traveling time-dependent deviation of the metric tensor, denoted by $h_{\mu\nu}$. We follow a common textbook development for the metric deviation of a gravitational wave, which finds that only the spatial components h_{ij} are nonzero, and further can be taken to be transverse and traceless [7]. The tensor is simplified if we initially write it in the "wave frame," denoted by primed coordinates and indices. It is a coordinate frame with its origin at the center of mass of the detector, and the z' axis aligned with the propagation direction of the wave. Since we restrict ourselves to detectors much smaller than the gravitational wavelength, only the time dependence of $h_{i'j'}$ will have significant physical effects. Thus, the most general possible form for the spatial components of the metric deviation in the wave frame can be written as

$$h_{i'j'}(t) = \begin{bmatrix} h'_+(t) & h'_\times(t) & 0 \\ h'_\times(t) & -h'_+(t) & 0 \\ 0 & 0 & 0 \end{bmatrix} , \qquad (1)$$

where h'_+ and $h'_\times$ are the wave amplitudes for the two allowed states of linear polarization, and are called the plus and cross amplitudes.

The detector is more easily described in the "laboratory frame," denoted by unprimed coordinates and indices, with its origin also at the center of mass of the detector, and z axis aligned with the local vertical. In this frame, the primary physical effect of a passing gravitational wave is to produce a time dependent "tidal" force density $f^{\mathrm{GW}}(x, t)$ on material at coordinate location x_i with mass density ρ, which is related to the metric perturbation by

$$f_i^{\mathrm{GW}}(x, t) = \frac{1}{2}\rho \sum_j \frac{\partial^2 h_{ij}(t)}{\partial t^2} x_j. \qquad (2)$$

We notice that this force can be written as the gradient of a time-dependent scalar potential:

$$f_i^{\mathrm{GW}}(x, t) = \nabla_i \Phi(x, t) = \nabla_i \left(\sum_{j,k} \frac{1}{4}\rho x_j \ddot{h}_{jk}(t) x_k \right) . \qquad (3)$$

This scalar potential is a quadratic form in the spatial coordinates. It is natural to look for an alternate expression that separates the coordinate dependence into radial and angular parts. Because the tensor h_{ij} is traceless, the angular expansion can be done completely with the five ordinary spherical harmonics of order 2, which we denote by $Y_m(\theta, \phi)$ or Y_m. We call the resulting time dependent expansion coefficients, denoted by $h_m(t)$, the "spherical amplitudes." They are a complete and orthogonal representation of the Cartesian metric deviation tensor $h_{ij}(t)$. They depend only on the two wave-frame amplitudes and the direction of propagation, and are defined by

$$\Phi(x, t) = \sqrt{\frac{\pi}{15}}\rho r^2 \sum_m \ddot{h}_m(t) Y_m. \qquad (4)$$

We have found it convenient to use a set of spherical harmonics Y_m that are linear combinations of the usual complex-valued spherical harmonics Y_{2m}. We define them by

$$Y_1 = \sqrt{\frac{1}{2}}\left(Y_{22} + Y_{2-2}\right) = \sqrt{\frac{15}{16\pi}}\frac{\left(x^2 - y^2\right)}{r^2} , \qquad (5a)$$

$$Y_2 = \sqrt{\frac{1}{2}}i\left(Y_{2-2} - Y_{22}\right) = \sqrt{\frac{15}{16\pi}}\frac{2xy}{r^2} , \qquad (5b)$$

$$Y_3 = \sqrt{\frac{1}{2}}\left(Y_{21} + Y_{2-1}\right) = \sqrt{\frac{15}{16\pi}}\frac{2yz}{r^2} , \qquad (5c)$$

$$Y_4 = \sqrt{\frac{1}{2}}i\left(Y_{2-1} - Y_{21}\right) = \sqrt{\frac{15}{16\pi}}\frac{2xz}{r^2} , \qquad (5d)$$

$$Y_5 = Y_{20} = \sqrt{\frac{15}{16\pi}}\frac{\left(3z^2 - r^2\right)}{r^2\sqrt{3}} . \qquad (5e)$$

They are normalized such that $\int Y_m \cdot Y_n d\Omega = \delta_{mn}$.

To transform the metric perturbation to the laboratory frame we perform the appropriate rotations, using the y convention of the Euler angles [8]. Ordinarily, without making any assumptions about the source, we do not know the initial state of the polarizations; we may therefore ignore the rotation about the original z' axis because this rotation only mixes the two polarizations and has no

effect in determining the direction of the wave. We denote the rotation about the y' axis by β and the rotation about the new z axis by γ. The spherical amplitudes can now be written in terms of the gravitational wave amplitudes:

$$h_1(t) = h'_+(t)\tfrac{1}{2}\left(1 + \cos^2\beta\right)\cos 2\gamma + h'_\times(t)\cos\beta\sin 2\gamma ,$$
(6a)

$$h_2(t) = -h'_+(t)\tfrac{1}{2}\left(1 + \cos^2\beta\right)\sin 2\gamma + h'_\times(t)\cos\beta\cos 2\gamma ,$$
(6b)

$$h_3(t) = -h'_+(t)\tfrac{1}{2}\sin 2\beta\sin\gamma + h'_\times(t)\sin\beta\cos\gamma ,$$
(6c)

$$h_4(t) = h'_+(t)\tfrac{1}{2}\sin 2\beta\cos\gamma + h'_\times(t)\sin\beta\sin\gamma ,$$
(6d)

$$h_5(t) = h'_+(t)\tfrac{1}{2}\sqrt{3}\sin^2\beta .$$
(6e)

If the laboratory x axis points south and the laboratory z axis is the local zenith, then the source has a zenith distance $= \beta$ and an azimuth (degrees east of north along the horizon) $= \gamma$.

The five orthogonal spherical amplitudes h_m are the complete set of measurable quantities of the local gravitational field. The determination of the source direction follows immediately by inversion of Eq. (6). Explicit formulas for this can be found in work soon to be published [9,10]. The position determination is only unique within a hemisphere; sources in opposite directions are indistinguishable.

III. THE GENERAL ANTENNA

The mechanics of a general antenna can be described by ordinary elastic theory. Forces acting on the body will cause a deformation described by the displacement vector $\boldsymbol{u}(\boldsymbol{x},t)$, where $\boldsymbol{x}$ is the equilibrium position of a mass element. The equations of motion are then

$$\rho\frac{\partial^2\boldsymbol{u}}{\partial t^2} = (\lambda + \mu)\boldsymbol{\nabla}(\boldsymbol{\nabla}\cdot\boldsymbol{u}) + \mu\boldsymbol{\nabla}^2\boldsymbol{u} + \sum\boldsymbol{f} ,$$
(7)

where the Lamé coefficients λ and μ specify the elastic stiffness of the material and $\sum\boldsymbol{f}$ represents the sum of external force densities acting on the body [11].

In this paper we include two forces in $\sum\boldsymbol{f}$. First, the signal or gravitational force density $\boldsymbol{f}^{\mathrm{GW}}$ from Eq. (2). Second, if objects are attached to the antenna, there will exist a reaction force between the object and the surface of the antenna. Thus we choose to express the coupling to other objects, such as secondary resonators, as if they were external forces in Eq. (7). This device lets us partition the equations of motion in a convenient way.

A solution to the differential equation (7) can be found by the standard eigenfunction expansion. This allows a separation of the spatial and time dependence of the displacement vector:

$$\boldsymbol{u}(\boldsymbol{x}_i,t) = \sum_m a_m(t)\boldsymbol{\Psi}_m(\boldsymbol{x}_i).$$
(8)

Each spatial eigenfunction, $\boldsymbol{\Psi}_m(\boldsymbol{x})$, is the time independent part of the solution for unforced harmonic oscillation at the eigenfrequency ω_m, and is found by solving

$$-\rho\omega_m^2\boldsymbol{\Psi}_m = (\lambda + \mu)\boldsymbol{\nabla}(\boldsymbol{\nabla}\cdot\boldsymbol{\Psi}_m) + \mu\boldsymbol{\nabla}^2\boldsymbol{\Psi}_m,$$
(9)

subject to the time-stationary boundary conditions, which for a sphere require that the total force per unit area at the surface vanish in the direction normal to the surface. The quantity $a_m(t)$ is the time-dependent mode amplitude. The mode index m enumerates the discrete set of modes, which obey the usual orthogonality property

$$\int_V \boldsymbol{\Psi}_m(\boldsymbol{x})\cdot\boldsymbol{\Psi}_n(\boldsymbol{x})d^3x = N_m\delta_{mn}.$$
(10)

The normalization constant N_m is arbitrary.

Combining the equations above, and using orthogonality to eliminate the summation, we find the standard result, one forced harmonic oscillator equation for each mode amplitude:

$$\ddot{a}_m(t) + \omega_m^2 a_m(t) = \frac{1}{\rho N_m}\int\boldsymbol{\Psi}_m(\boldsymbol{x})\cdot\sum\boldsymbol{f}(\boldsymbol{x},t)d^3x.$$
(11)

When comparing different calculations, one source of possible confusion is the arbitrary choice of normalization constant N_m. It determines the units and the precise physical interpretation of both the mode amplitudes a_m and the eigenfunctions $\boldsymbol{\Psi}_m$.

The mode amplitudes are a complete set of collective coordinates for the description of the antenna motion. All the interactions with the outside world, including gravitation, can be included as separate terms in the "effective force" on each mode. An efficient approximation scheme will use only those modes needed for an accurate description of the antenna. Only a few of the "overlap integrals" with $\boldsymbol{f}^{\mathrm{GW}}$ in Eq. (11) are large, so that only a few of the mode amplitudes are strongly coupled to gravitational waves.

IV. THE UNCOUPLED SPHERE

Let us consider a perfectly homogeneous and isotropic sphere uncoupled from the outside world. Its eigenfunctions were found over a hundred years ago by Jaerisch [12] and Lamb [13]. More elegant derivations, using modern notation, were found by Ashby and Dreitlein [14], and Wagoner and Paik [3]. We summarize their results.

The eigenfunctions of a sphere can be described in terms of spherical harmonics $Y_{\ell m}(\theta,\phi)$. Looking at the overlap integral in Eq. (11) we see that we need only consider odd-parity modes. For a sphere of radius R the eigenfunctions are written

$$\boldsymbol{\Psi}_{\ell m} = [\alpha_\ell(r)\hat{\boldsymbol{r}} + \beta_\ell(r)R\boldsymbol{\nabla}]Y_{\ell m}(\theta,\phi),\quad \ell \text{ even}.$$
(12)

The radial eigenfunctions $\alpha_\ell(r)$ and $\beta_\ell(r)$ determine the motion in the radial and tangential directions, respectively. There are five quadrupole modes of vibration which strongly couple to the force density of a gravitational wave, and are all degenerate, having the same angular eigenfrequency ω_o. They are distinguished only
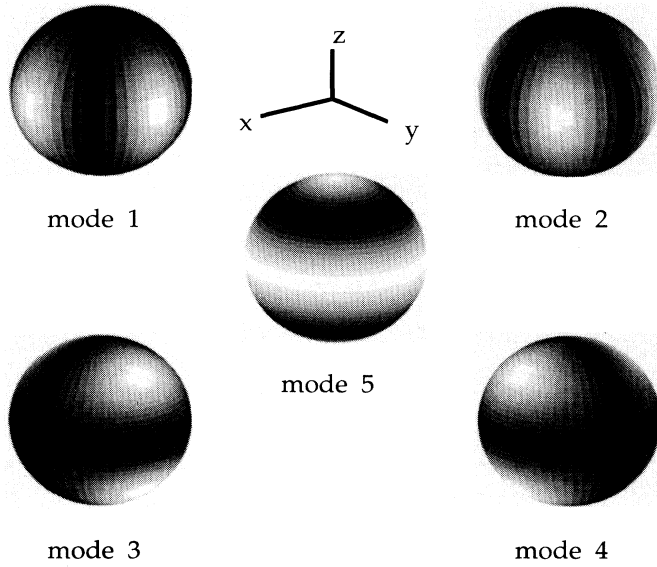
FIG. 1. The shape of the quadrupole modes. The shading indicates the amplitude of radial motion. The dark regions have little or no radial motion; the lightest regions have the maximum of radial motion.

by their angular dependence. Figure 1 shows the shape of the quadrupole modes. For the remainder of this discussion we will only consider the quadrupole ($\ell = 2$) modes so we will drop the ℓ in our notation.

The radial eigenfunctions are given by Ashby and Dreitlein:

$$\alpha(r) = cR\frac{\partial}{\partial r}j_2(qr) + 6dR\frac{1}{r}j_2(kr) , \tag{13}$$

$$\beta(r) = cj_2(qr) + d\frac{\partial}{\partial r}[rj_2(kr)] . \tag{14}$$

Their dependence on Poisson's ratio is shown in Fig. 2.

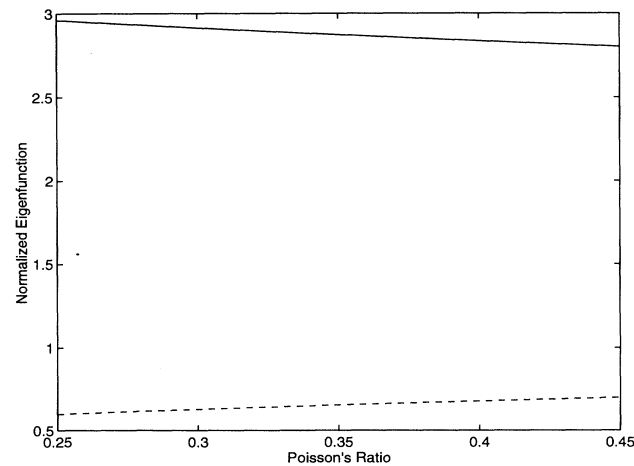FIG. 2. The value of the normalized eigenfunctions, α (solid line) and β (dotted line), at the sphere surface, as functions of Poisson's ratio.
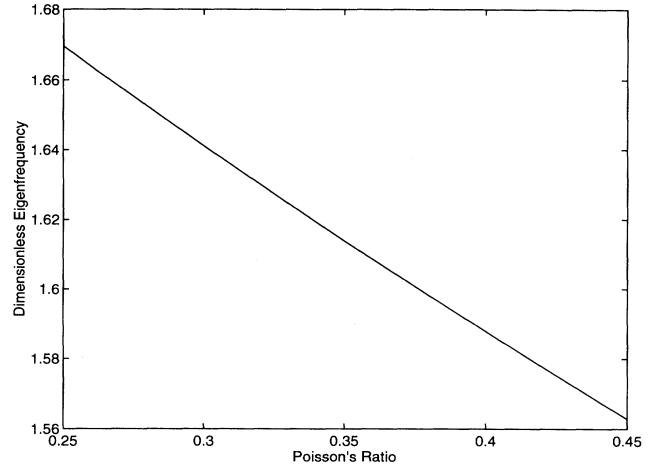

FIG. 3. The dimensionless eigenfrequency of the uncoupled quadrupole modes of a sphere, $\omega_0 R\sqrt{\frac{\rho}{E}}$, as a function of Poisson's ratio.

j_2 is the spherical Bessel function of order 2. The longitudinal and transverse wave vectors are given by $q^2 = \rho\omega_0^2/(\lambda + 2\mu)$ and $k^2 = \rho\omega_0^2/\mu$, respectively. The boundary conditions

$$c\frac{d}{dr}\left[\frac{j_2(qr)}{r}\right] + d\left[\frac{5}{r^2} - \frac{k^2}{2} - \frac{1}{r}\frac{d}{dr}\right]j_2(kr)\Bigg|_{r=R} = 0, \tag{15}$$

$$c\left[\frac{6}{r^2} - \frac{k^2}{2} - \frac{2}{r}\frac{d}{dr}\right]j_2(qr) + 6d\frac{d}{dr}\left[\frac{j_2(kr)}{r}\right]\Bigg|_{r=R} = 0 \tag{16}$$

determine the uncoupled mode frequency ω_0. Its dependence on Poisson's ratio is shown in Fig. 3. Inclusion of a normalization condition
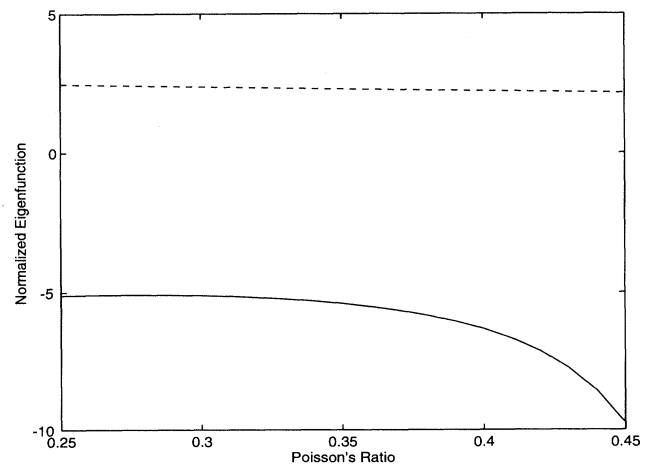

FIG. 4. The normalized eigenfunctions c (solid line) and d (dotted line) as functions of Poisson's ratio.
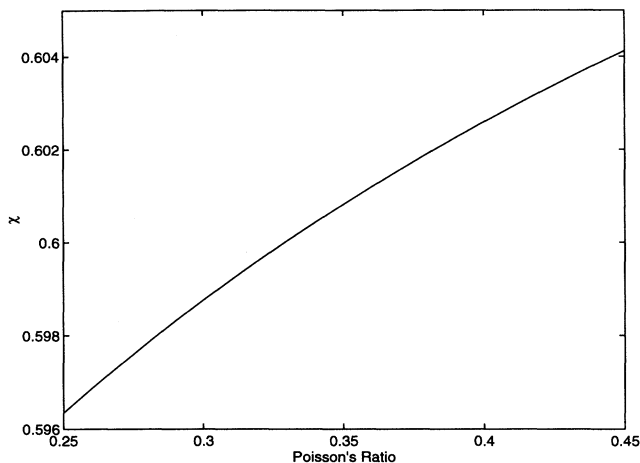
FIG. 5. The fraction χ, which determines the effective length of the sphere, as a function of Poisson's ratio.

$$N_m \equiv \tfrac{4}{3}\pi R^3 \tag{17}$$

determines the constants c and d. These coefficients specify the shape of the eigenfunctions. They are all weakly dependent on Poisson's ratio, as shown in Fig. 4.

The gravitational effective force for mode m of the sphere F_m^S, from Eq. (11) is

$$F_m^S \equiv \int_{V_0} \boldsymbol{\Psi}_m \cdot \boldsymbol{f}^{\mathrm{GW}}\, d^3x. \tag{18}$$

Solving the integrals, using Eqs. (3) and (12) we find

$$
\begin{aligned}
F_m^S(t) &= \sqrt{\frac{4\pi}{15}}\,\rho \ddot{h}_m(t) R^4 \left[c j_2\left(qR\right) + 3 d j_2\left(kR\right) \right] \\
&= \frac{1}{2}\ddot{h}_m(t)\, m_S\, \chi R.
\end{aligned}
\tag{19}
$$

Thus we have that each spherical component of the gravitational field determines uniquely the effective force on the corresponding mode of a sphere, and they are all identical in magnitude. We can interpret the effective force F_m^S in each mode as the product of the physical mass of the sphere m_S, an effective length χR, and the gravitational acceleration $\frac{1}{2}\ddot{h}_m$. The factor χ is a weak function of Poisson's ratio, and is shown in Fig. 5.

V. SPHERE WITH RESONATORS

A. Equations of motion

We have just shown that measurement of the quadrupole modes of a sphere measures all of the spatial dependence of the gravitational field, but a simple spherical resonator is not a practical detector. As mentioned in the Introduction, one requirement for practicality is a set of secondary modes or mechanical resonators. All current bar antennas use resonators that interact only with the

vector component of antenna motion normal to the surface on which they are mounted. Thus it seems natural to restrict our consideration to resonators of this type. The alternate possibility, interaction with transverse components of the antenna motion, is under consideration by others [9].

Designate the location of each resonator j by $\boldsymbol{x}_j$. Then the normal displacement, z_j, of the sphere surface under resonator j, is given by

$$z_j(t) = \hat{\boldsymbol{r}}_j \cdot \sum_m a_m(t)\boldsymbol{\Psi}_m\left(\boldsymbol{x}_j\right). \tag{20}$$

By mechanical resonator we mean a small elastic system that has one of its own normal modes tuned to be resonant with the frequency of the antenna. The antenna surface motion excites this mode, and there is resonant transfer of momentum between the resonator and the antenna. Hence it acts as a resonant mechanical transformer, turning small motions of the large antenna into large motions of the small resonator. Each resonator j is constructed to obey a one-dimensional harmonic oscillator equation:

$$m_R\left[\ddot{q}_j(x_j,t) + \ddot{z}_j(x_j,t)\right] = -k_R q_j(x_j,t) + F_j^N(x_j,t). \tag{21}$$

The displacement of the resonator, relative to the sphere surface, is denoted by q_j. Because q_j is a relative displacement, the inertial displacement of the resonator mass is $q_j + z_j$, hence the peculiar form for the left-hand side of the equation above. Each resonator is assumed identical, and the mass m_R and spring constant k_R of each are tuned to match the frequency of the five sphere modes so that $k_R/m_R = \omega_o^2$. Any random or noise forces that act between the small resonator and the sphere are included in F_j^N. A schematic of the one-dimensional system is shown in Fig. 6.

The values of the relative radial displacements of the sphere surface, at the resonator locations, can be grouped
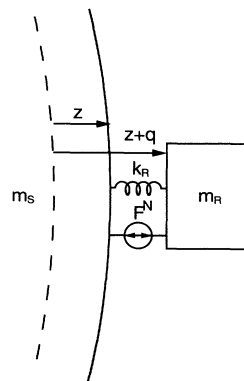

FIG. 6. Schematic of a one-dimensional resonator attached to the surface of a sphere.

together into a "pattern vector" for a particular mode, because they describe the pattern of radial displacement for that mode. These column vectors in turn may be collected together to form a "pattern matrix" B_{jm} defined by

$$\hat{r}_j \cdot \boldsymbol{\Psi}_m (x_j) = \alpha B_{mj} \qquad (22)$$

where $\alpha = \alpha(R)$. From Eq. (12) we find

$$B_{mj} = Y_m (\theta_j, \phi_j). \qquad (23)$$

Because the wave functions are invariant to reflection through the origin, we may restrict the location of resonators to one hemisphere, without loss of generality.

Combining the above, we find the coupled equations of motion for the sphere modes are

$$m_S \ddot{a}_m(t) + k_S a_m(t)$$

$$= \sum_j \alpha B_{mj} \left[k_R q_j(t) - F_j^N(t) \right] + F_m^S(t). \qquad (24)$$

It is convenient to combine Eqs. (21) and (24) into a matrix notation. We denote matrices by a double underline and column vectors by a single underline:

$$\begin{bmatrix} m_S \underline{\underline{I}} & \underline{\underline{0}} \\ m_R \alpha \underline{\underline{B}}^T & m_R \underline{\underline{I}} \end{bmatrix} \begin{bmatrix} \ddot{\underline{a}}(t) \\ \ddot{\underline{q}}(t) \end{bmatrix} + \begin{bmatrix} k_S \underline{\underline{I}} & -k_R \alpha \underline{\underline{B}} \\ \underline{\underline{0}} & k_R \underline{\underline{I}} \end{bmatrix} \begin{bmatrix} \underline{a}(t) \\ \underline{q}(t) \end{bmatrix}$$

$$= \begin{bmatrix} \underline{\underline{I}} & -\alpha \underline{\underline{B}} \\ \underline{\underline{0}} & \underline{\underline{I}} \end{bmatrix} \begin{bmatrix} \underline{F}^S(t) \\ \underline{F}^N(t) \end{bmatrix}. \qquad (25)$$

The vector $\underline{a}$ has 5 components and the vector $\underline{q}$ has 1 component for each resonator. The dimensions of the constant matrices can be inferred from these two column vectors.

These equations should give an excellent account of the mechanics of the system for arbitrary numbers and locations of resonators. They are restricted only by the previously stated assumptions: degeneracy for the uncoupled sphere modes and precise matching of the resonators. Most of the new features of a multimode spherical antenna are included, particularly the strong interactions between the sphere modes and the resonators. We have not included terms which represent the "dissipation" part of friction, which can be shown to be negligible for the sensitivity calculations we do here. We do include the "fluctuation" part of friction, within the random driving forces in $\underline{F}^S$ and $\underline{F}^N$.

It is clear that these equations represent a set of elastically coupled harmonic oscillators with driving forces. The apparent peculiarities (off-diagonal terms in the mass matrix and asymmetry in the elastic matrix) are simply artifacts of use of the noninertial coordinates q. In the Appendix we show how to transform them into the canonical normal form, with normal coordinates η:

$$\ddot{\underline{\eta}}(t) + \omega_0^2 \underline{\underline{D}} \, \underline{\eta}(t) = \underline{\underline{U}}^T \underline{\underline{K}} \, \underline{F}(t). \qquad (26)$$

The sphere overlap integrals and the resonator noise forces are contained in the column vector $\underline{F}$. $\underline{\underline{U}}^T$ is the transpose of a set of eigenvectors that diagonalize the equations. The matrix $\underline{\underline{D}}$ is the diagonal matrix of eigenvalues for the normal modes described by $\underline{\underline{U}}$, and $\underline{\underline{K}}$ is a constant transformation matrix. The equations of motion are now in a form that can easily be solved numerically using standard techniques.

To solve for the resonator displacements q and sphere mode amplitudes $\underline{a}$ we take the Fourier transform of equation (26), and solve for $\eta(\omega)$. Once the normal coordinates have been found, the sphere mode amplitudes and resonator displacements are found by a constant transformation.

B. Truncated icosahedral arrangement

We can solve the equations above for arbitrary numbers and locations of small resonators, and determine whatever quantities are interesting, such as the coupled eigenfrequencies and eigenvectors. One important question is whether there exists any favored or optimum arrangement.

By a simple counting argument we expect that a minimum of five resonators are required to completely measure the five quadrupole modes of the sphere, so our initial calculations considered the frequency structure with five resonators tuned to the frequency of the degenerate sphere modes.

The eigenmodes of the coupled system are naturally split up and down in frequency. From earlier work on optimizing a bar antenna coupled to a single resonator [4], we knew that the amount of frequency splitting was an indicator of the strength of the coupling, and normally would need to be adjusted to a particular value to optimize the overall signal to noise ratio. Therefore we were disappointed to discover that the 10 coupled modes did not split in an identical way. For every arrangement of five transducers that we tried, we found that the resulting coupled modes were arranged in singlets, doublets, and triplets, each with a different splitting from the original common frequency.

We then tried six resonators and quickly discovered that there was an arrangement that greatly simplified the frequency structure: it became two degenerate quintuplets and a singlet. The geometric location of the resonators was found to be precisely the projection, onto the sphere, of the centers of half the faces of a concentric dodecahedron.

A truncated icosahedron (TI) has the same point group symmetries as a dodecahedron [15], but better approximates a sphere. It also has 32 flat surfaces suitable for mounting transducers, calibrators, balancing weights, and suspension attachments. Therefore, we proposed to use six pentagonal faces of a TI, instead of a dodecahedron, for arranging the mechanical resonators [6]. This shape, with the proposed resonator locations, is shown in Fig. 7.

The high symmetry of the TI arrangement becomes apparent when you examine its pattern matrix. Each

pattern vector is orthogonal to the others, and each has the same magnitude, $\sqrt{\frac{3}{2\pi}}$, or, in other words,

$$\underline{\underline{B}}\,\underline{\underline{B}}^T = \frac{3}{2\pi}\underline{\underline{I}}. \tag{27}$$

This property causes the cross terms between sphere modes in the eigenfunctions to vanish, having the effect of isolating each sphere mode from the others. Without this, the energy from an excitation of a single sphere mode would end up "leaking" into the other sphere modes through the mechanical resonators. This allows us to use the sphere modes as a direct measurement of the gravitational spherical amplitudes.

In addition to the orthogonality, the sum of the components of each pattern vector vanishes, or

$$\underline{\underline{B}}\underline{1} = \underline{0}. \tag{28}$$

(The 6×1 column vector $\underline{1}$ is defined to have all elements equal to unity, while the 5×1 column vector $\underline{0}$ has all elements equal to zero.) This property will allow us to easily remove from our analysis the lone mode, which does not interact with a gravitational wave.

Since discovering this arrangement, we have not considered others in comparable detail. We have not attempted to make a proof that it is the optimum arrangement, but its symmetry leads us to conjecture that such a proof will be discovered.

C. Analytic solution

The symmetry of the pattern matrix also suggested that there might be an analytic solution for the collection of eigenvectors $\underline{\underline{U}}$ and the eigenvalue matrix $\underline{\underline{D}}$ of Eq. (26). Examination of the numerical results suggested a likely form for $\underline{\underline{U}}$, and substitution in the equations verified that it was a solution and determined the values of the constants. The details of this solution are found in
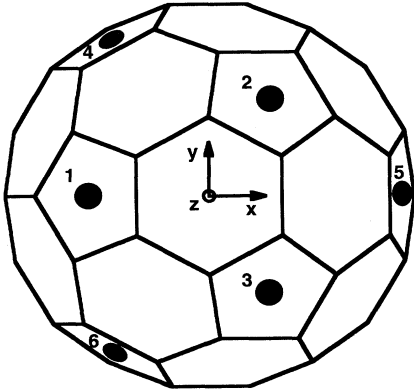

FIG. 7. The truncated icosahedral gravitational wave antenna (TIGA) with secondary resonator locations indicated. The resonators lie at two polar angles, $\theta = 37.3773°$ and $79.1876°$. Their azimuthal angles are multiples of $60°$, as shown. The numbering on the resonators corresponds to the order used in the numerical simulation of Sec. V E.

the Appendix.

It is convenient to divide the resulting set of eigenvectors $\underline{\underline{U}}$ into three groups. The first two groups each contain five column eigenvectors and we denote them by $\underline{\underline{U}}_+$ and $\underline{\underline{U}}_-$:

$$\underline{\underline{U}}_\pm = n_\pm \left[\begin{array}{c} \underline{\underline{I}} \\ c_\pm \underline{\underline{B}}^T \end{array} \right]. \tag{29}$$

The physical interpretation of these is simple: each coupled eigenmode "mimics" the motion of one of the uncoupled sphere eigenmodes. In other words, each coupled resonator's radial motion is proportional to the uncoupled sphere wave function at that resonator's location. This amplified version of a mode's pattern vector is either in phase (downshifted in frequency) or antiphase (upshifted in frequency). The frequency shifts are all identical, so that the quintuplet of degenerate bare sphere-modes has bifurcated into upshifted and downshifted degenerate quintuplets of modes. The amount of frequency shifting is given by the eigenvalues, $\lambda_\pm$, which are the diagonal elements of the matrix $\underline{\underline{D}}$. The identity matrix in the sphere components of the eigenvectors is an indication that energy will *not* be transferred from one sphere mode to another. The $\pm$ notation has been used on the constants $n_\pm$ and $c_\pm$ as well as to refer to the up ($+$) or down ($-$) shifting of the frequencies.

The remaining single eigenvector is

$$\underline{\underline{U}}_0 = \left[\begin{array}{c} \underline{0} \\ n_0 \underline{1} \end{array} \right]. \tag{30}$$

This mode is at the original sphere frequency and does not interact with a gravitational wave. All the resonators move in unison and the sphere modes do not move at all.

The five dimensionless constants $n_\pm$, $c_\pm$, and n_o can be determined using the Hermitian property of the transformation, $\underline{\underline{U}}^T\underline{\underline{U}} = \underline{\underline{I}}$. The symmetry properties of the pattern matrix, Eqs. (27) and (28), play an important role here to simplify the work involved in determining these constants and in calculating the eigenvalues. We summarize the results:

$$n_\pm^2 = \frac{1}{1 + \frac{3}{2\pi}c_\pm^2}, \quad n_0^2 = \frac{1}{6}, \tag{31}$$

$$c_\pm = -\frac{1}{2}\left(b \pm \sqrt{b^2 + \frac{8\pi}{3}} \right), \tag{32}$$

$$\lambda_\pm = 1 + \frac{3}{4\pi}b\left(b \pm \sqrt{b^2 + \frac{8\pi}{3}} \right), \quad \lambda_0 = 1, \tag{33}$$

where $b \equiv \alpha\sqrt{m_R/m_S}$. The relative splitting of the coupled modes is given by $\Delta\omega/\omega_0 = \sqrt{\lambda_+} - \sqrt{\lambda_-} \simeq 1.98\sqrt{m_R/m_S}$ for a Poisson's ratio of 0.36.

D. Mode channels

In an experiment, the measured quantities are the resonator amplitudes $q_j(t)$. Since they mimic the motion

of the sphere, most of them are excited when only one sphere mode is excited. It would be helpful to have a direct way to determine the spherical amplitudes $h_m(t)$.

We have discovered that we can separate out each of the spherical amplitudes by forming fixed linear combinations of the measured amplitudes $q_j(t)$. We call these combinations "mode channels," to indicate that each one is coupled only to a single mode amplitude, $a_m(t)$, of the uncoupled sphere, and hence to a single amplitude $h_m(t)$ of the gravitational field. The linear combination desired for a given mode turns out to be the pattern vector for that mode. Therefore, if we denote the five desired outputs as a column vector $\underline{g}$, they are given by

$$\underline{g}(t) \equiv \underline{\underline{B}}\,\underline{q}(t). \tag{34}$$

The analytic solution of the complete system is most simply expressed in the frequency domain. Taking that solution from the Appendix, and using Eq. (34) we find that each mode channel Fourier amplitude $g_m(\omega)$ is linearly related to the forces by Eq. (A16), which is

$$g_m(\omega) = \sigma(\omega)F_m^S(\omega) + \sum_j H_{mj}(\omega)F_j^N(\omega). \tag{35}$$

The response function $\sigma(\omega)$ is a scalar, so that each mode channel $g_m(\omega)$ responds only to the corresponding spherical component $F_m^S(\omega)$ and hence only to the corresponding gravitational component $h_m(\omega)$. In addition, $\sigma(\omega)$ has the same frequency dependence as that of a bar-type antenna with one secondary resonator, so we can adopt familiar methods for parameter adjustment and time-series filtering.

In contrast, each mode channel responds to all the internal noise forces $F_j^N(\omega)$, via the matrix response function $H_{mj}(\omega)$. So the noise observed in one channel will be a superposition of the noises generated in all the resonators.

E. Numerical simulation of the TIGA system

The first major result of this paper is that all the readout complications mentioned in the Introduction are solved by using the mode channels. We illustrate this with a numerical simulation for two cases. We are only interested in demonstrating the mode channel concept, so we omit any noise terms from this simulation. For the first case, Fig. 8 shows the response of the five sphere modes $\underline{a}$ to the tidal force of a gravitational wave burst, which arrives at $t = 0$, propagating along the z axis with $h_\times$ its only nonzero amplitude. The only nonzero force component is F_2, so only the a_2 component of the sphere modes is excited. The special symmetry of the TI arrangement prevents transfer of excitation to the other sphere modes, so they remain unexcited.

The measurable quantities, the resonator displacements $\underline{q}$, are shown in Fig. 9. To determine the sphere mode amplitudes from the observables $\underline{q}$ we multiply by the pattern matrix to obtain the mode channels $\underline{g}$. Figure 10 shows the result of this calculation. By comparing
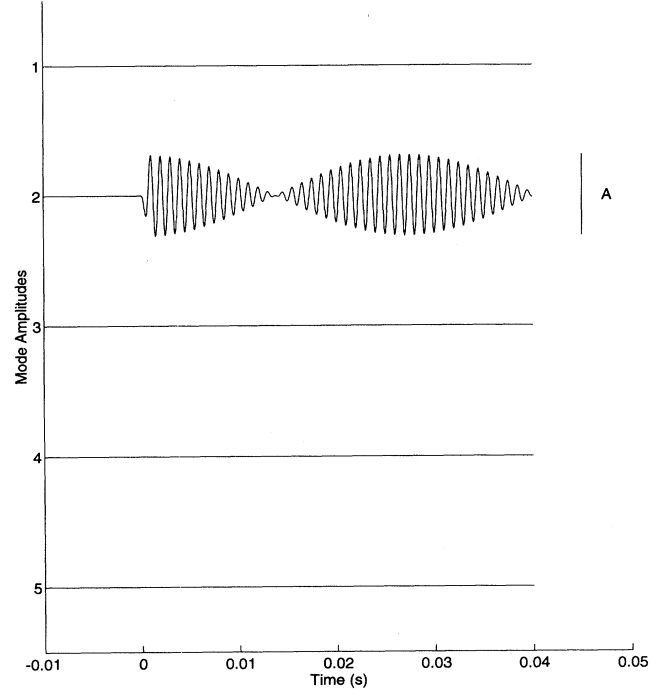

FIG. 8. The response of the five sphere mode amplitudes $\underline{a}$ to the first simulated case of a gravitational wave burst of arbitrary size at $t = 0$, propagating along the z axis with only nonzero amplitude $h_\times$. The scale bar to the right indicates the maximum amplitude A of the sphere mode, for comparison with Fig. 9.
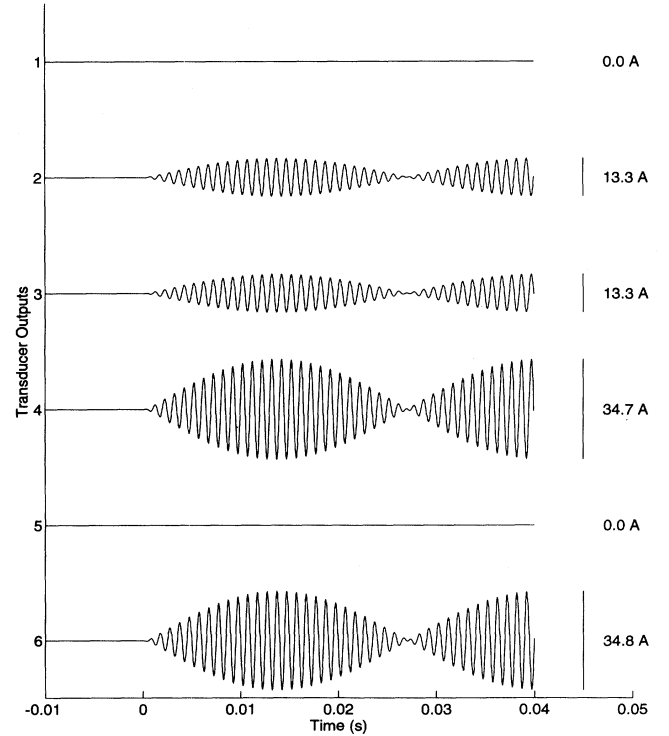

FIG. 9. The resonator displacements $\underline{q}$ due to the burst of the first simulated case. The scale bars to the right indicates the maximum displacement of each resonator, relative to the sphere amplitude A of Fig. 8.
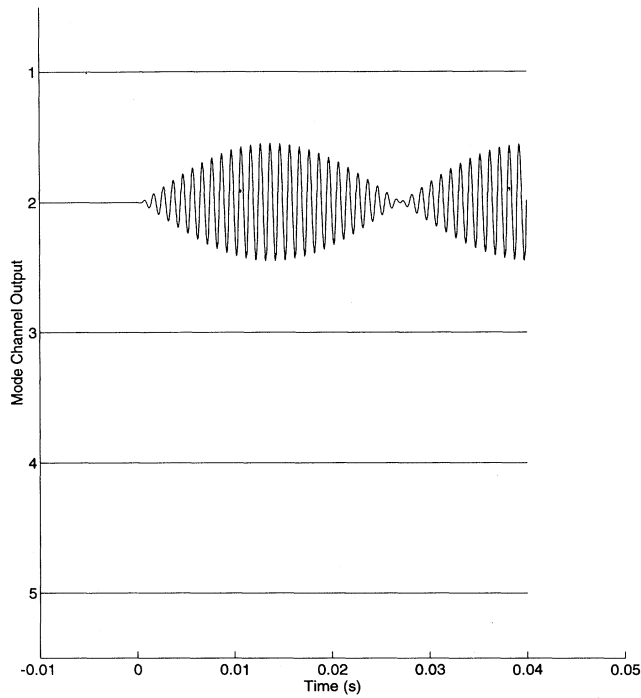
FIG. 10. The mode channels $\underline{g}$ calculated from the resonator displacements of Fig. 9 for the first simulated case.
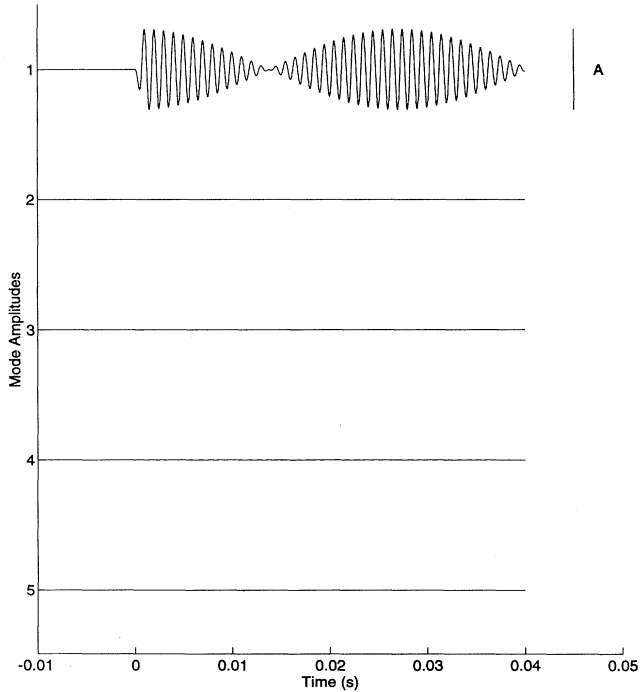
FIG. 11. The response of the five sphere mode amplitudes $\underline{a}$ to the second simulated case of a gravitational wave burst of arbitrary size at $t = 0$, propagating along the z axis with only nonzero amplitude h_+. The scale bar to the right indicates the maximum amplitude A of the sphere mode, for comparison with Fig. 12.
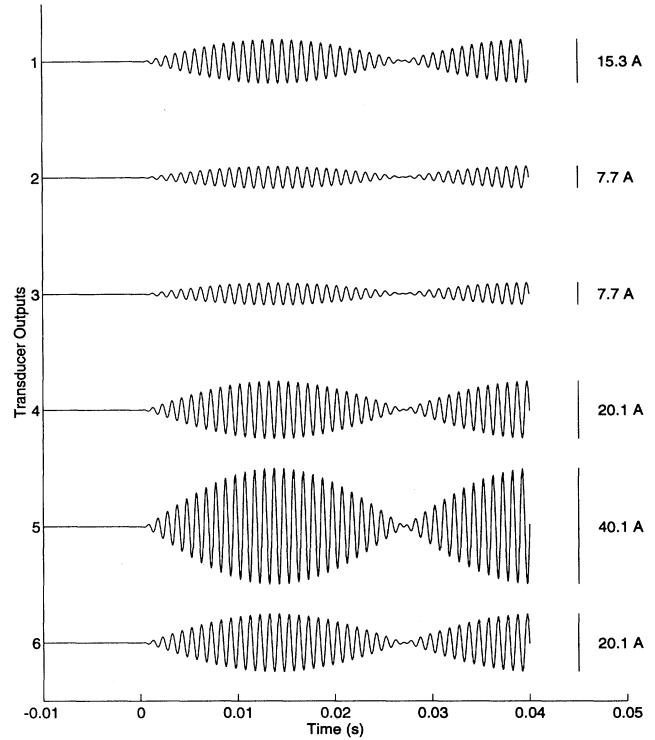
FIG. 12. The resonator displacements $\underline{q}$ due to burst of the second simulated case. The scale bars to the right indicates the maximum displacement of each resonator, relative to the sphere amplitude A of Fig. 11.
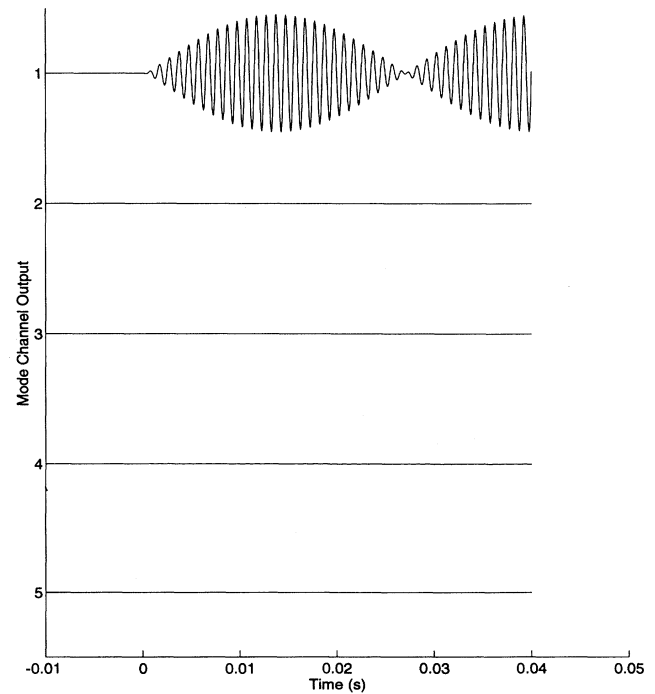
FIG. 13. The mode channels $\underline{g}$ calculated from the resonator displacements of Fig. 12 for the second simulated case.

Fig. 10 to Fig. 8, it is obvious that (except for a phase shift of the envelope) the mode channels give a direct, one-to-one, readout of the sphere mode amplitudes, and thus of the gravitational wave.

For the second case, Figs. 11, 12, and 13 show the results of the above calculation repeated for a gravitational wave burst propagating along the z axis with amplitude h_+.

VI. SPECTRAL SENSITIVITY

We have found above a set of equations for the system and a method of solution. We can now apply them to predict the sensitivity of a model detector. First, we write down the response of each mode channel $g_m(\omega)$ to the gravitational wave input $h_m(\omega)$. From Eqs. (19) and (35),

$$g_m(\omega) = -\tfrac{1}{2}\omega^2 m_S \sigma(\omega)\chi R h_m(\omega) \; . \tag{36}$$

Second, we model the noise sources and calculate the system response to them. We have chosen to use a simple noise model which includes only two categories of noise certain to be important: (1) displacement noise, or random voltages in the electronic readout of the mechanical displacement q and (2) force noise, or random forces that actually excite the mechanical system. We assume both are generated in what Price [16] calls the "mechanical amplifiers," or the transducer-amplifier combinations, which convert the resonator motions q into an electronic readout. The displacement noise has a spectral density denoted by $S^q(\omega)$.

The force noise caused by the transducer-amplifier combination will appear as a random term in $F_j^N(\omega)$. We denote its spectral density as $S^F(\omega)$. We leave out of this model all of the Langevin noise forces that can be important with nonzero temperatures and nonzero mechanical losses, thus we are calculating the generalization of Giffard's limit [17] for a multimode multitransducer antenna without mechanical losses.

These two noise sources can also be represented in a different way, by defining a "noise number" and a "noise resistance" for each transducer amplifier. The noise number N is the amplifier noise temperature T_n referred to the quantum of energy at the antenna frequency:

$$N \equiv \frac{k_b T_n}{\hbar\omega} = \sqrt{\frac{S^F S^q}{\hbar^2}}. \tag{37}$$

The noise resistance is defined by

$$r_n \equiv \sqrt{\frac{S^F}{\omega^2 S^q}}. \tag{38}$$

It is a measure of the strength of the electromechanical coupling in the transducer-amplifier combination.

Combining the above and transforming using Eq. (34) and the noise part of Eq. (35) we find that the calculated noise spectrum at the mode channel g_m is

$$S_m^g(\omega) = S^F(\omega) \sum_j |H_{mj}(\omega)|^2 + S^q(\omega) \sum_j |B_{mj}|^2 \; . \tag{39}$$

We assume the noise generators are all statistically independent.

Finally, we must compare the signal and noise responses, using some criterion for detectability. This final step can be done in a number of ways. For these calculations we have chosen to use a method not used before with resonant detectors, but now commonly used with laser interferometer gravitational wave detectors.

We calculate $\tilde{h} = \sqrt{S_h}$, the gravitational "strain spectrum" or "spectral sensitivity." It is the square root of the total noise spectral density measured at the output, in this case g_m, referred back to the gravitational inputs h_m. It quantifies the fictitious gravitational background noise that would be required to mimic the stationary random output of the antenna. Assuming only stationary noise is present, it has the advantage of allowing comparison of different types of antennas. It also can be used to determine the signal-to-noise ratio for any specified signal waveform.

The noise spectral density of each mode channel g_m, referred back to the corresponding spherical component h_m is therefore

$$S_m^h(\omega) = \frac{4k_b T_n}{\omega^4 R^2 m_S^2 \chi^2} \frac{r_n \left| \frac{\beta_+}{\omega_+^2 - \omega^2} + \frac{\beta_-}{\omega_-^2 - \omega^2} \right|^2 + \frac{m_S m_R}{r_n \omega^2}}{\left| \frac{\alpha_+}{\omega_+^2 - \omega^2} + \frac{\alpha_-}{\omega_-^2 - \omega^2} \right|^2}$$
$$\times \sum_j |B_{mj}|^2 \; , \tag{40}$$

where $\alpha_\pm$ and $\beta_\pm$ are dimensionless constants found in the Appendix.

From Eq. (40) we see that the calculated strain spectrum is proportional to the square root of the noise number. The shape of the strain noise is prescribed by the noise resistance r_n and the mode splitting. Figure 14 shows the strain noise for noise number, $N = 1$, for a 1 kHz aluminum TIGA. The three solid lines are for different values of the noise resistance.

VII. COMPARISON OF THE TIGA TO OTHER DETECTORS

It is possible to construct a number of TIGA's at different frequencies to create a "xylophone." Doing so would enable one to partially determine the waveform of an incoming gravitational wave. The spectral density of a range of TIGA sizes is shown in Fig. 15. The resonator to sphere mass ratio and noise resistance were adjusted to give consistent fractional bandwidth and a maximally flat curve. Parameters of this xylophone are shown in Table I.

For comparison, the corresponding results for the equivalent bars, optimally oriented (bar axis orthogonal to an incoming wave), for the same strain component are shown as dashed lines in Fig. 15. The strain noise $\tilde{h}^B$, with $N = 1$, for the equivalent bar is larger by a factor of 3.9.

The second important result of this paper is that for equivalent conditions (equal noise numbers), a single
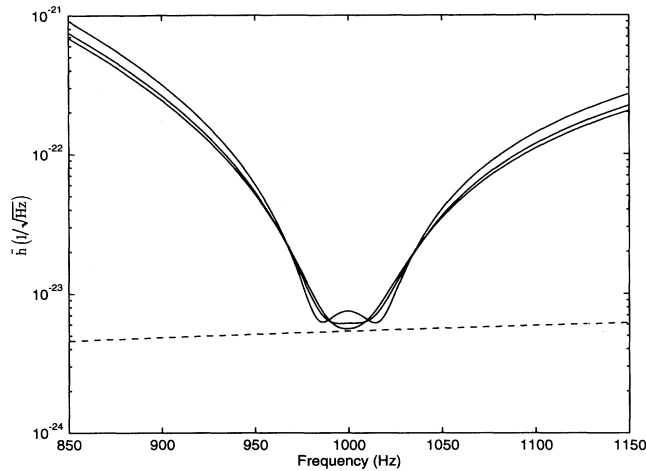
FIG. 14. The strain noise spectrum $\tilde{h}(\omega) = \sqrt{S_h}$ for a single mode channel of a 1 kHz aluminum TIGA with noise number $N = 1$, for three different values of the noise resistance r_n. The dotted line is the additional noise due to the Langevin forces for an antenna at 50 mK with a mechanical quality factor of 10^8.

channel of a TIGA will have $3.9^2 = 15$ times better energy resolution than the optimally oriented equivalent bar. This is nearly the same improvement calculated by scaling up the mass of the bar by this amount, so we conclude that a single channel of the TIGA suffers no signal-to-noise penalty due to the various complications in the readout.
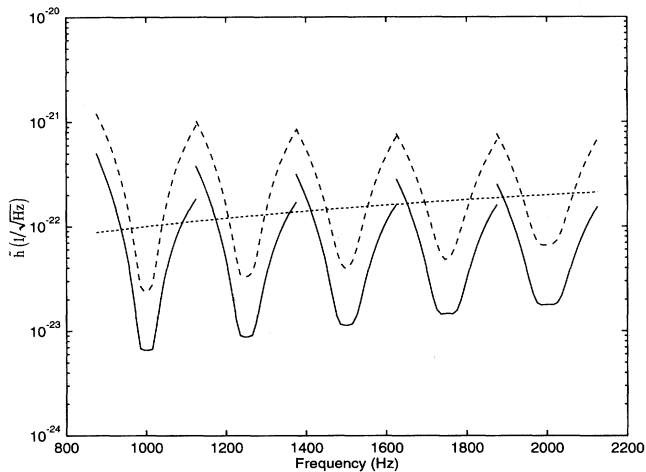

FIG. 15. The calculated strain noise spectrum $\tilde{h}(\omega) = \sqrt{S_h}$ for various detectors. The solid lines are a "xylophone" of TIGA detectors with quantum limited sensor noise, for a single channel (i.e., a single linear polarization arriving from an arbitrary direction). The dashed lines are a xylophone of equivalent bar antennas with quantum limited sensor noise, for the optimum orientation of the wave. The dotted line is the first generation Laser Interferometric Gravitational Wave Observatory (LIGO) detector, for the optimum orientation of the wave [18].

TABLE I. Parameters for the "xylophone" of TIGA detectors shown as the solid lines in Fig. 15. The material is aluminum.

Frequency (Hz)	Radius (m)	Sphere mass (kg)	Transducer mass (kg)
1000	1.30	25100	9.02
1250	1.04	12800	4.62
1500	0.87	7400	2.67
1750	0.74	4700	1.68
2000	0.65	3100	1.13

The comparisons in Fig. 15 understate the overall advantage of the TIGA for the detection of gravitational waves. The five output channels combined make the detector optimally oriented for any polarization and incident direction. For a bar detector, it is well known that averaging over source direction and polarization [7] leads to a loss of energy resolution, compared to the optimum, by a factor of $15/4 = 3.7$. Thus the net result is that the angle-averaged energy resolution of the TIGA is $3.7 \times 15 = 56$ times better than the equivalent bar detector (or about 7.5 times better in h).

Also shown for comparison in Fig. 15 (dotted line) is the predicted strain noise for the first generation LIGO detector [18] in its most favorable orientation for the same signal. It is evident that a xylophone of quantum limited TIGA's is significantly more sensitive over most of this frequency range, even without considering the extra information available about orientation. However, the predicted LIGO strain noise continues to drop, proportional to frequency, down to ~ 100 Hz. We conclude that the two detector types are complementary, each having a frequency domain where the predicted sensitivities are superior. In addition to covering different frequencies, each uses two different technologies, which is advantageous when confirming tentative detection of a gravitational wave.

By creating a xylophone of TIGA's, they are no longer limited to being narrow-band detectors. The "notes of the scale" can provide substantial spectral information about the detected wave. Coherent recording of the outputs will allow relative phase measurement, hence partial reconstruction of the time dependence of the waveform.

VIII. EXTENSIONS

Our noise model omitted the Langevin forces due to finite temperature and mechanical damping. In current practice, these are very significant. The inclusion of resonator damping will add a contribution to the random forces F_j^N, which will have the effect of increasing the noise number and the noise resistance so that their effect is immediately calculable via Eq.(40).

The inclusion of antenna damping will add noise terms to the effective forces F_m^S on the sphere modes. Because they act at the same point as the gravitational inputs, it is simple to calculate their spectral densities, referred to h_m. The single sided spectral density of the Langevin force is well known to be

$$S^Q = 4k_bT\frac{m_S\omega}{Q}, \tag{41}$$

where Q is the mechanical quality factor of the sphere, T is the physical temperature, and k_b is the Boltzmann constant. Using Eq. (19) we refer this force to the gravitational input in Fig. 14. The dashed line shows the noise for a TIGA with a $Q = 10^8$ at 50 mK. Clearly if one can obtain a high enough Q, the noise in the system due to antenna damping can be ignored.

A natural extension of this work would be to calculate the effect of small departures from the perfect symmetry and perfect matching assumed here. We want to know if orthogonal mode channels be constructed, and also how much will the sensitivity degrade? Our experience with somewhat similar departures from perfect matching (such as the frequency mistuning of a resonator on a bar antenna) suggest that the sensitivity is affected only in second order by small departures of a parameter from its optimum value [19], but a quantitative calculation of these effects will be of practical interest for construction of such an antenna.

Another extension would be a calculation of the effect of adding a resonant transducer for the first monopole mode of the sphere, because it potentially provides a detector for scalar gravitational waves, which may be of theoretical interest.

Other possible extensions include: multimode resonators, and additional resonators to monitor a higher frequency harmonic of the quadrupole modes.

ACKNOWLEDGMENTS

APPENDIX

The equations of motion for a sphere with resonators are given by Eq. (25). We simplify this equation by making a number of transformations. First, we transform the resonator displacements and sphere amplitudes into the 11 mass weighted coordinates $\underline{w}$:

$$\begin{bmatrix} \underline{a} \\ \underline{q} \end{bmatrix} = \underline{\underline{\gamma}}\,\underline{w} \equiv \begin{bmatrix} \frac{1}{\sqrt{m_S}}\underline{\underline{I}} & \underline{\underline{0}} \\ \underline{\underline{0}} & \frac{1}{\sqrt{m_R}}\underline{\underline{I}} \end{bmatrix}\underline{w}. \tag{A1}$$

Next, we remove the matrix multiplying the second time derivatives by multiplying both sides of the equation by its inverse. We end up with the equation

$$\ddot{\underline{w}} + \omega_0^2 \begin{bmatrix} \underline{\underline{I}} & -\sqrt{\frac{m_R}{m_S}}\alpha\underline{\underline{B}} \\ -\sqrt{\frac{m_R}{m_S}}\alpha\underline{\underline{B}}^T & \left(\underline{\underline{I}} + \frac{m_R}{m_S}\alpha^2\underline{\underline{B}}^T\underline{\underline{B}}\right) \end{bmatrix}\underline{w}$$

$$= \frac{1}{\sqrt{m_S}} \begin{bmatrix} \underline{\underline{I}} & -\alpha\underline{\underline{B}} \\ -\sqrt{\frac{m_R}{m_S}}\alpha\underline{\underline{B}}^T & \sqrt{\frac{m_R}{m_S}}\left(\frac{m_S}{m_R}\underline{\underline{I}} + \alpha^2\underline{\underline{B}}^T\underline{\underline{B}}\right) \end{bmatrix}$$

$$\times \begin{bmatrix} \underline{F}^S \\ \underline{F}^N \end{bmatrix}, \tag{A2}$$

which is of the form $\ddot{\underline{w}} + \omega_0^2\underline{\underline{M}}\,\underline{w} = \underline{\underline{K}}\,\underline{F}$. The matrix $\underline{\underline{M}}$ is symmetric; therefore, it can be diagonalized by the transformation $\underline{\underline{U}}^T\underline{\underline{M}}\,\underline{\underline{U}} = \underline{\underline{D}}$ where $\underline{\underline{U}}$ is a set of eigenvectors, and $\underline{\underline{D}}$ is the diagonal matrix of the eigenvalues of $\underline{\underline{M}}$. Substituting this in Eq. (A2) and multiplying by $\underline{\underline{U}}^T$ we get

$$\ddot{\underline{\eta}} + \omega_0^2\underline{\underline{D}}\,\underline{\eta} = \underline{\underline{U}}^T\underline{\underline{K}}\,\underline{F}, \tag{A3}$$

where $\underline{\eta}$ are now our normal coordinates. The problem has now been reduced to 11 decoupled harmonic oscillator equations that can easily be solved in a number of different ways. We begin by taking the Fourier transform of Eq. (A3):

$$\underbrace{\left(-\omega^2\underline{\underline{I}} + \omega_0^2\underline{\underline{D}}(\omega)\right)}_{\underline{\underline{G}}^{-1}(\omega)}\underline{\eta}(\omega) = \underline{\underline{U}}^T\underline{\underline{K}}\,\underline{F}(\omega). \tag{A4}$$

Because $\underline{\underline{D}}(\omega)$ is diagonal, $\underline{\underline{G}}^{-1}(\omega)$ is diagonal, so its inverse is just the diagonal elements inverted. The normal coordinates are

$$\underline{\eta}(\omega) = \underline{\underline{G}}(\omega)\underline{\underline{U}}^T\underline{\underline{K}}\,\underline{F}(\omega)\,. \tag{A5}$$

To return to the original coordinates we reverse the transformations:

$$\begin{bmatrix} \underline{a}(\omega) \\ \underline{q}(\omega) \end{bmatrix} = \underline{\underline{\gamma}}\,\underline{\underline{U}}\,\underline{\eta}(\omega) = \underline{\underline{\gamma}}\,\underline{\underline{U}}\,\underline{\underline{G}}(\omega)\underline{\underline{U}}^T\underline{\underline{K}}\,\underline{F}(\omega). \tag{A6}$$

For the TI arrangement, the eigenvectors $\underline{\underline{U}}$ have the form given in Eqs. (29) and (30), with the result that the matrices become

$$\underline{\underline{\gamma}} = \begin{bmatrix} \frac{1}{\sqrt{m_S}}\underline{\underline{I}} & \underline{\underline{0}} \\ \underline{\underline{0}} & \frac{1}{\sqrt{m_R}}\underline{\underline{I}} \end{bmatrix}, \tag{A7}$$

$$\underline{\underline{K}} = \frac{1}{\sqrt{m_S}} \begin{bmatrix} \underline{\underline{I}} & -\alpha\underline{\underline{B}} \\ -b\underline{\underline{B}}^T & \sqrt{\frac{m_S}{m_R}}\left(\underline{\underline{I}} + b^2\underline{\underline{B}}^T\underline{\underline{B}}\right) \end{bmatrix}, \tag{A8}$$

$$\underline{\underline{U}} = \begin{bmatrix} n_+\underline{\underline{I}} & n_-\underline{\underline{I}} & \underline{\underline{0}} \\ n_+c_+\underline{\underline{B}}^T & n_-c_-\underline{\underline{B}}^T & n_0\underline{\underline{1}} \end{bmatrix}, \tag{A9}$$

$$\underline{\underline{G}}(\omega) = \begin{bmatrix} \frac{1}{(\omega_+^2-\omega^2)}\underline{\underline{I}} & \underline{\underline{0}} & \underline{\underline{0}} \\ \underline{\underline{0}} & \frac{1}{(\omega_-^2-\omega^2)}\underline{\underline{I}} & \underline{\underline{0}} \\ \underline{\underline{0}} & \underline{\underline{0}} & \frac{1}{(\omega_0^2-\omega^2)} \end{bmatrix}, \tag{A10}$$

where $b \equiv \alpha\sqrt{m_R/m_S}$ and $n_\pm$, $c_\pm$, and n_o are given in Eqs. (31)–(33). To simplify further we define

$$\alpha_\pm \equiv \frac{3}{2\pi}n_\pm^2 c_\pm\left(1 - \frac{3}{2\pi}c_\pm b\right), \tag{A11}$$

$$\beta_\pm \equiv \frac{3}{2\pi}n_\pm^2 c_\pm\sqrt{\frac{m_S}{m_R}}\left[-b + c_\pm\left(1 + \frac{3}{2\pi}b^2\right)\right], \tag{A12}$$

$$\omega_\pm^2 \equiv \lambda_\pm\omega_0^2. \tag{A13}$$

After some algebra we find the resonator displacements and sphere mode amplitudes to be given by

$$\underline{a}(\omega) = \frac{2\pi}{3m_S}\left(\frac{\alpha_+/c_+}{\left(\omega_+^2 - \omega^2\right)} + \frac{\alpha_-/c_-}{\left(\omega_-^2 - \omega^2\right)}\right)\underline{F}^S(\omega) + \frac{2\pi}{3m_S}\left(\frac{\beta_+/c_+}{\left(\omega_+^2 - \omega^2\right)} + \frac{\beta_-/c_-}{\left(\omega_-^2 - \omega^2\right)}\right)\underline{\underline{B}}\,\underline{F}^N(\omega), \tag{A14}$$

$$\underline{q}(\omega) = \frac{2\pi}{3\sqrt{m_S m_R}}\left(\frac{\alpha_+}{\left(\omega_+^2 - \omega^2\right)} + \frac{\alpha_-}{\left(\omega_-^2 - \omega^2\right)}\right)\underline{\underline{B}}^T\,\underline{F}^S(\omega)$$

$$+ \left[\frac{2\pi}{3\sqrt{m_S m_R}}\left(\frac{\beta_+}{\left(\omega_+^2 - \omega^2\right)} + \frac{\beta_-}{\left(\omega_-^2 - \omega^2\right)}\right)\underline{\underline{B}}^T\,\underline{\underline{B}} + \frac{1}{6m_R\left(\omega_0^2 - \omega^2\right)}\underline{\underline{1}}\right]\underline{F}^N(\omega). \tag{A15}$$

To convert the resonator displacements to mode channels we need only multiply by the pattern matrix $\underline{\underline{B}}$. In the frequency domain, the mode channels, in terms of the noise forces, are given by the remarkably simple expression

$$\underline{g}(\omega) = \frac{1}{\sqrt{m_S m_R}}\left(\frac{\alpha_+}{\left(\omega_+^2 - \omega^2\right)} + \frac{\alpha_-}{\left(\omega_-^2 - \omega^2\right)}\right)\underline{F}^S(\omega)$$

$$+ \frac{1}{\sqrt{m_S m_R}}\left(\frac{\beta_+}{\left(\omega_+^2 - \omega^2\right)} + \frac{\beta_-}{\left(\omega_-^2 - \omega^2\right)}\right)\underline{\underline{B}}\,\underline{F}^N(\omega) \tag{A16}$$

$$\equiv \sigma(\omega)F_m^S(\omega) + \sum_j H_{mj}(\omega)F_j^N(\omega). \tag{A17}$$

[1] W. O. Hamilton, in *Sixth Marcel Grossmann Conference on General Relativity and Gravitation*, Proceedings, Kyoto, Japan, 1991, edited by H. Sato and T. Nakamura (World Scientific, Singapore, 1992).

[2] R. Forward, Gen. Relativ. Gravit. **2**, 149 (1971).

[3] R. V. Wagoner and H. J. Paik, in *Proceedings of International Symposium on Experimental Gravitation, Pavia* (Roma Accademia Nazionale dei Lincei, Roma, 1976), pp. 257–265.

[4] P. F. Michelson and R. C. Taber, J. Appl. Phys. **52**, 4313 (1981).

[5] P. F. Michelson and R. C. Taber, Phys. Rev. D **29**, 2149 (1984).

[6] W. W. Johnson and S. M. Merkowitz, Phys. Rev. Lett. **70**, 2367 (1993).

[7] K. S. Thorne, in *Three Hundred Years of Gravitation*, edited by S. W. Hawking and W. Israel (Cambridge University Press, Cambridge, England, 1987), Chap. Gravitational Radiation.

[8] H. Goldstein, *Classical Mechanics*, 2nd ed. (Addison-Wesley, Reading, Massachusetts, 1980).

[9] Z. Zhou, Ph.D. thesis, Stanford University, 1994; C. Zhou and P. F. Michelson, Phys. Rev. D **51**, 2517 (1994).

[10] N. S. Magalhães, W. W. Johnson, C. Frajuca, and O. D. Aguiar, Mon. Not. R. Astron. Soc. (to be published).

[11] L. D. Landau and E. M. Lifshitz, *Theory of Elasticity*, 3rd ed. (Pergamon, New York, 1986).

[12] P. Jaerisch, J.f. Math. (Crelle) **Bd. 88** (1880).

[13] H. Lamb, in *Proceedings of the London Mathematical Society* (1882), Vol. 13.

[14] N. Ashby and J. Dreitlein, Phys. Rev. D **12**, 336 (1975).

[15] P. Pearce and S. Pearce, *Polyhedra Primer* (Van Nostrand Reinhold, New York, 1978).

[16] J. C. Price, Phys. Rev. D **36**, 3555 (1987).

[17] R. P. Giffard, Phys. Rev. D **14**, 2478 (1976).

[18] A. Abramovici *et al.*, Science **256**, 325 (1992).

[19] N. Solomonson, W. W. Johnson, and W. O. Hamilton, Phys. Rev. D **46**, 2299 (1992).
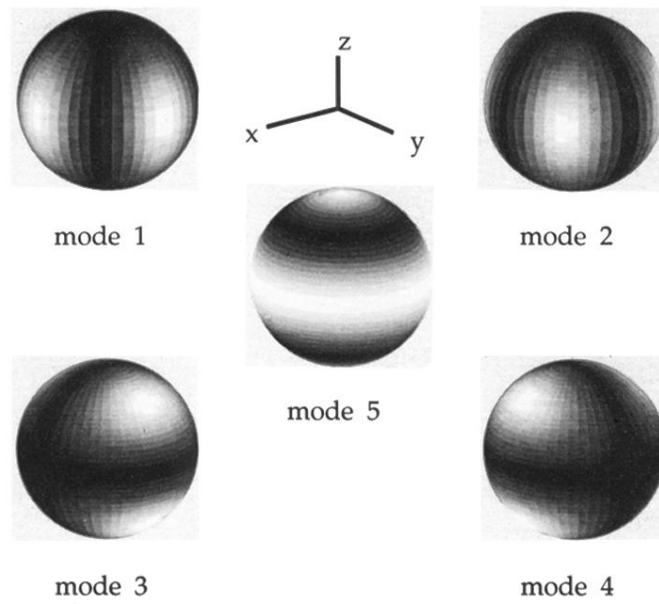
FIG. 1. The shape of the quadrupole modes. The shading indicates the amplitude of radial motion. The dark regions have little or no radial motion; the lightest regions have the maximum of radial motion.